POLISH MARITIME RESEARCH 4 (128) 2025 Vol. 32; pp. 157-167
10.2478/pomr-2025-0059

Early-Stage Investigation of Environmentally Friendly Sliding Bearings for Offshore Wind Turbine Main Shafts

Filip Wasilczuk*
Institute of Fluid Flow Machinery, Polish Academy of Sciences, Fiszera 14 St., Gdańsk, Poland
Michał Wasilczuk
Gdańsk University of Technology, Faculty of Mechanical Engineering and Ship Technology, 11/12 Narutowicza St., Gdańsk, Poland
Paweł Flaszyński
Institute of Fluid Flow Machinery, Polish Academy of Sciences, Fiszera 14 St., Gdańsk, Poland
Wojciech Litwin
Gdańsk University of Technology, Faculty of Mechanical Engineering and Ship Technology, 11/12 Narutowicza St., Gdańsk, Poland

* Corresponding author: *fwasilczuk@imp.gda.pl (Filip Wasilczuk)*

ABSTRACT

This work presents a preliminary assessment of the potential application of water-lubricated radial sliding bearings as main shaft bearings in large offshore wind turbines. The study is driven by the environmental concerns and the high cost and size associated with conventional rolling element bearings. Four bearing material candidates were examined: lignum vitae, a compliant elastic polymer, a three-layer PTFE-based composite, and a fibre-reinforced polymer. Pilot experiments were carried out on a custom-built test rig capable of accurately capturing friction torque under controlled radial loads, with freshwater serving as both lubricant and coolant. The procedure included a defined running-in phase and multiple repeated tests to ensure reproducibility. The sliding speed and load conditions were determined using a combination of multi-body dynamic simulations of the IEA 15 MW reference turbine and published load analyses, ensuring that the test conditions reflect realistic operating values. The results showed that the polymer and PTFE-based composite exhibited excellent tribological behaviour, maintaining very low friction coefficients during both steady and start-up operation. Although the wear behaviour was not quantified at this stage, the low friction coefficients indicate operation in a full hydrodynamic lubrication regime, which is expected to minimise wear. Overall, this preliminary investigation suggests that selected water-lubricated sliding bearings represent a promising, environmentally friendly alternative for offshore wind turbine main shafts, offering advantages in corrosion resistance, durability under dynamic loading, and potentially low wear.

Keywords: wind turbine bearing, low-speed sliding bearing, energy efficiency, journal bearings experimental tests

INTRODUCTION

The development of offshore wind farms, particularly those exceeding 15 MW in capacity, introduces complex engineering challenges. These turbines feature massive rotors with diameters over 200 m and main shafts up to 2.5 m in diameter, designed to withstand substantial mechanical loads. Traditionally, rolling element bearings have been used in wind turbine drivetrains, including gearboxes and main shafts. A thorough review of the state of the art in wind turbine drive systems and their bearings is presented by Nejad et al. [1]. However, as turbine dimensions and power ratings increase, rolling bearings face significant limitations. Their manufacturing becomes more difficult and expensive at larger scales, and their performance under extreme operating conditions – such as low rotational speeds below 0.2 m/s and system weights exceeding 500 tons – often leads to premature failures [2]. These failures are frequently attributed to fatigue, misalignment, and wear mechanisms that are not yet fully understood; a good state-of-the-art review can be found in [3].

It is worth noting that rolling element bearings are one of the most failure-prone components of wind turbines. An analysis conducted by Hart et al. [4] based on the operational data from over 7000 turbines shows that over 20% of the bearings do not withstand 20-year operation, as they are designed to do, with 10% requiring replacement after only 10.5 years. This replacement is expensive and non-trivial, causing a significant increase in the operating cost and a loss of energy production. Examples from wind energy and other applications show that the discrepancy between the predicted operation life and reality may result from issues such as the following:

– a turbine operating outside of design limits [5];
– bearing misalignment [6];
– the unseating, sliding, and skewing of the rolling elements due to a high axial-to-radial-load ratio [7, 8];
– debris accumulation [9].

Sliding bearings can offer several advantages in wind turbine drivetrains, particularly under conditions of high dynamic loading and large shaft diameters. Their continuous surface contact allows superior load distribution and shock absorption compared to rolling bearings, making them especially suitable for main shaft [10] and planetary gear applications [11]. Additionally, sliding bearings exhibit lower noise and vibration levels, and their simpler design can reduce maintenance complexity and costs. These benefits are particularly pronounced under hydrodynamic and mixed lubrication regimes, where sliding bearings demonstrate enhanced damping and wear resistance [12, 13]. According to general knowledge about the modes of failure of sliding bearings, one should expect mild abrasive wear under the conditions of operation in the wind turbine, especially during starts and stops, when the full film lubrication regime is not possible due to a low sliding speed. Contrary to rolling element bearings' modes of failure, this form of failure develops gradually over time.

Recent research has focused on optimising sliding bearing designs to meet the demands of high-power wind turbines [14]. Innovations such as tailored radial clearances and axial crowning have shown promise in reducing edge pressures and improving durability under thermo-hydrodynamic conditions. Compared to rolling bearings, sliding bearings exhibit no clear fatigue limit, better corrosion resistance, and more favourable wear debris characteristics. These attributes make them well-suited for the harsh and variable environments typical of offshore wind installations. As a result, sliding bearings are increasingly viewed not only as a substitute for rolling bearings but as a strategic advancement in drivetrain technology for next-generation wind turbines.

Over the years, the feasibility of applying sliding bearings to wind turbine main shafts has been well demonstrated, and they are now considered cutting-edge technology in this field; examples of recent research and application achievements are presented in [2]. Germany's RENK developed a 6 MW sliding bearing for wind turbine main shafts; it has been deployed in small batches and tested for 10 MW applications. Siemens and GE have developed prototype turbines in the 2–5 MW range using sliding bearings, and they have already been connected to the grid. In China, sliding bearings for wind turbine main shafts have been applied in a 2 MW unit at the Harbin Electric Equipment National Engineering Research Center. In 2021, another Chinese company successfully operated a 4 MW semi-direct drive turbine with sliding bearings at the Dabancheng Wind Farm in Xinjiang, achieving over 20% improvement in load-bearing density and a 60% reduction in maintenance costs.

This paper aims to experimentally investigate the performance of bearings with four different bushing materials in conditions representative of large-scale wind turbine operation. The conditions are derived based on a literature survey and aeroelastic simulations performed using HAWC2 code [15]. The other aim is to select materials suitable for water lubrication and to test them in water lubrication. This aim in turn is motivated by increasingly stringent regulations concerning environmental protection in marine-related industries. Since environmental protection is one of the main priorities in the construction and operation of ships and ocean technical facilities, it is assumed that offshore wind energy may soon be covered by regulations similar to those regarding shipping, such as Vessel General Permission (VGP) [16] and the Vessel Incidental Discharge Act (VIDA) [17]. The shipping regulations introduce ecologically sound technologies, including environmentally acceptable lubricants (EALs) and the use of water as a lubricant wherever lubrication is necessary. As a result, four different sliding bearing materials compliant with water lubrication were tested, as this design choice may become obligatory in the future.

Water-lubricated bearings have been in relatively well-documented use since the 1860s, when a special wood (lignum vitae) bearing was installed in a Great Eastern ship, launched in 1864 [18]. Another group of water-lubricated bearings are rubber bushings, which were patented in 1924 [18]. Later, significant achievements in engineering in the 20th century led to the use of improved new materials, such as special polymers, metal-based composites, multi-layer composites [19], and ceramic bearings. Despite their long history and development, it is estimated that only 5−6% of the 100,000 to 120,000 ships in operation worldwide use water-lubricated stern tube bearings [20], but this is likely to change because of the increasingly demanding environmental regulations mentioned above. Apart from the marine industry, water-lubricated bearings are used in hydropower, especially as radial bearings in vertical shaft turbines, where rubber, special polymers, and metals with solid lubricants are used [21].

The study is limited to the radial bearings; further studies on the feasibility of using sliding bearings as the main bearings of a wind turbine must address the problem of accommodating the thrust load, but appropriate thrust bearing concepts also exist, e.g. [22].

The main bearing in a wind turbine plays a critical role in supporting the rotor and transmitting loads to the tower. Its design must meet several stringent requirements to ensure reliability and durability [23]:

1. Load Capacity: The bearing must withstand complex loads, including axial, radial, and moment loads, resulting from wind forces and rotor dynamics. Rotor loading will be discussed in more detail in the following sections.
2. Fatigue Life: The bearing should have a fatigue life that meets or exceeds the turbine's design life, typically 20 years. The calculations are performed based on norms; however, studies have shown that field failure rates can be as high

as 15–30% at 20 years [24], indicating that the assumed models may not be accurate.
3. Lubrication and Sealing: Effective lubrication is essential to minimise friction and wear. Given the challenging operating conditions, including variable loads and environmental factors, the bearing design must incorporate robust sealing solutions to prevent contamination and retain lubricants, especially for offshore turbines, where any leakage causes the pollution of the ocean environment.
4. Stiffness and Alignment: Proper stiffness and alignment are necessary to maintain the integrity of the bearing under load. Misalignment can lead to improper bearing operation, increasing the risk of premature failure.
5. Temperature Management: The bearing must operate effectively within the temperature ranges encountered in the nacelle, necessitating materials and designs that can withstand thermal variations.

The aerodynamic loading on the blades is a result of the wind acting on the blades. On average, the rotor loading in the axial direction is usually tabulated as the thrust coefficient:

$$C_T = \frac{2T}{\rho A v^2} \tag{1}$$

where T is the thrust force acting on the rotor, ρ is the density of air, and v is the wind speed.

Since the wind turbine operates in environmental conditions, the loading acting on the rotating blades is highly unsteady. The source of this unsteadiness can be wind shear, turbulence [25], or yaw misalignment [26]. Depending on the source, the unsteadiness can have a stochastic or periodic character.

The main source of stochastic forces acting upon the rotor and increasing the fatigue loading is atmospheric turbulence. In the case of wind farm clusters, additional turbulence is generated within the turbine wake [27], which increases the fatigue loading in downstream turbines even further [28]. This increase depends on the conditions, especially the atmospheric stability [29].

Kenworthy et al. [9] showed the sensitivity of the bearing life on both shear (partly responsible for uneven rotor loading) and atmospheric turbulence, with the former having a larger impact on the bearing life.

The frequency of periodic loading is connected to the rotational speed of the rotor. For three-bladed wind turbines that have few defects, most of the loading variability is related to the 3P frequency, which corresponds to three times the rotor speed. Due to the non-uniform wind profile and tower interaction, the inflow conditions vary for each blade with the azimuthal position. This is especially important for large wind turbines, where the difference between the conditions at the bottom and top positions of the blade is the highest.

In the case of defects in the shaft or bearing, or if there is a discrepancy between how the different blades operate, additional variability of the 1P (rotation frequency) or 2P (double rotation frequency) frequencies may occur. Heege and Hemmelmann [30] compared the coupling deformation from measurements and multi-body simulation (MBS) for the GE 1.5XLE wind turbine. Their measurements showed a significant deformation variability of the 1P and 2P frequencies, indicating some geometry imperfections. This effect was replicated in the simulations using a deformed shaft. Comparing such a simulation with a simulation without deformation allows a better understanding of the magnitude of deformation variability resulting from periodic changes in loading. The loading variability amplitude in the case with a deformed shaft was approximately 4 times larger than the 3P variability caused by blade rotation.

Calculating how the rotor loading translates to the bearings is a complicated task. The bearing load depends on, among other things, the rotor loading, shaft stiffness, number of bearings, and seating configuration dimensions. In practice, researchers use multi-body aeroelastic simulations to determine the impact of the rotor load on the bearing load [7, 24, 31]. It was shown that the bearing load depends on the wind shear and turbulence intensity [24].

DETERMINATION OF FORCES ACTING ON THE MAIN BEARING

In order to be able to conduct experimental tests of selected sliding connections, it was necessary to assess the forces acting on the main bearings of offshore wind turbines. Therefore, the impact of the wind on the turbine rotor was analysed, and then, the loads to which the main bearing may be subjected were calculated. The drivetrain design has a large impact on the bearing loads; however, the goal of this work is not to design a new drivetrain that includes sliding bearings but to test their viability for large-scale wind turbines. Thus, no particular layout of the drivetrain was considered at this stage.

In order to assess the loads, to later apply them in the test section, a reference wind turbine was selected, as all the data needed for this study are publicly available. The IEA 15 MW Reference Wind Turbine model (seen in Fig. 1) was selected from the reference wind turbine models available because its power is in line with that of the largest modern wind turbines that are currently being installed commercially. As mentioned before, for such large rotors, the mass and price of the rolling element bearings are very large, and hydrodynamic bearings may be an attractive alternative.

The main goal of this work is to study the viability of hydrodynamic bearings for large offshore wind turbines, with a focus on forces during startup. A model of the IEA 15 MW Reference Wind Turbine (RWT) created using the aeroelastic code HAWC2 [15] was used to assess the forces acting on the main bearing.

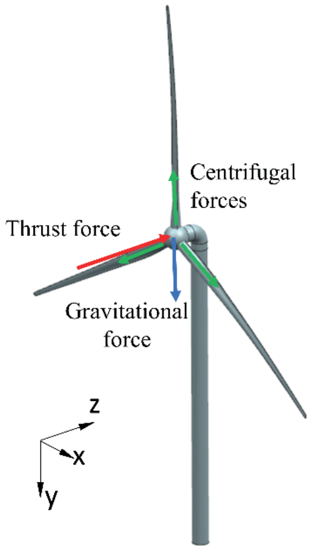

Fig. 1. The schematics of the IEA 15 MW turbine with the definition of the coordinate system

The database of the IEA 15MW wind turbine [32] contains rotor characteristics created using WISDEM code [33] that used idealised steady-state conditions and control aimed at power maximisation. Three sets of boundary conditions were determined from the characteristics. For wind speeds below 7 m/s, the turbine operates at 5 RPM. The rotational velocity translates to the velocity between the pad and the runner, which is a key parameter for a hydrodynamic bearing. If it is too low, the hydrodynamic effect is not sufficient, which may lead to failures, because of seizure or abrasive wear. Thus, the first set of operating conditions was based on the state where the rotor loading is largest for a 5 RPM rotational velocity, which is 7 m/s. The second wind speed condition investigated was 10.7 m/s, for which, according to the thrust curve shown for the turbine operating conditions (Fig. 2), the thrust force is the largest. The last set of conditions was based on turbine operation for very high wind speeds. The cut-off speed for the IEA 15 MW turbine is 25 m/s, but a wind speed of 24 m/s was selected, so that the turbine does not work too close to conditions that would cause it to shut down.

The aforementioned velocities were set at hub height. The power wind profile according to the IEC 61400-1 norm was used:

$$\frac{u}{u_r} = \left(\frac{z}{z_r}\right)^{\alpha} \tag{2}$$

where
u – the wind speed at height z;
u_r – the wind speed at reference height z_r;
– the reference height (hub height);
α – an empirically derived exponent (0.2 according to [34]).

A 3D coherent turbulence field was generated using the Mann turbulence box method [35] implemented in the Mann.rs tool [36]. The turbulence intensity was calculated using the following equation for the normal turbulence model from the IEC 61400-1 standard [34]:

$$TI = \frac{I_{ref}\left(0.75 \cdot u_r + 5.6\frac{m}{s}\right)}{u_r} \tag{3}$$

where
I_{ref} – the reference turbulence intensity, equal to 0.16 according to [34]. Wind turbine class A was assumed, as it is the worst-case loading scenario.
u_r – the wind speed at hub height.

Table 1 presents a summary of the configurations for the computed cases. The simulations presented here use the DTU Basic Controller, available in HAWC2 [37]. The selected conditions are unsteady, and the controller takes into account the turbine safety margin, which may lead to changes in turbine settings in the model. Table 1 shows the time-averaged HAWC2 model results compared with rotor characteristics obtained from the IEA 15MW Reference Wind Turbine database [32]. The thrust forces for the models for the same wind speed are comparable, showing that the HAWC2 simulations are trustworthy.

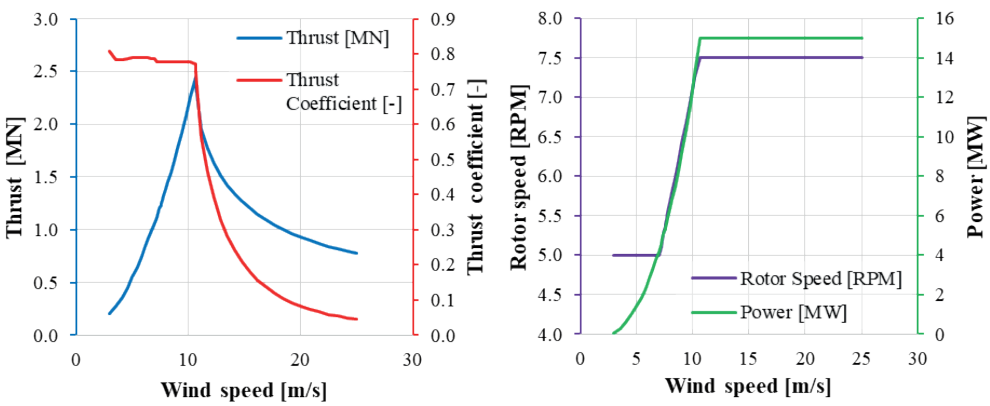

Fig. 2. Thrust force, thrust coefficient (CT), rotor speed, and power for IEA 15 MW RWT

Tab. 1. Wind turbine operating parameters for analysed configurations

	WISDEM			HAWC2			
Wind speed	**Rotational speed**	**Thrust**	**Power**	**Rotational speed**	**Thrust**	**Power**	**TI**
m/s	RPM	MN	MW	RPM	MN	MW	-
7	5.0	1	4.2	5.7	1.2	6.8	0.25
10.7	7.5	2.45	15	7.6	1.8	15.5	0.20
24.0	7.5	0.8	15	7.6	0.8	15.6	0.16

The forces on each of the axes were determined using HAWC2, according to the model definition presented above. Unsteady conditions are posed at the inlet (using the Mann turbulence box), resulting in an unsteady force. Thus, the results for each case were averaged, and the standard deviation was computed for 15 rotor revolutions (Table 2).

Tab. 2. Wind turbine operating parameters for analysed configurations

	WS = 7 m/s			WS = 10.7 m/s			WS = 24.0 m/s		
	Fx [kN]	Fy [kN]	Fz [kN]	Fx [kN]	Fy [kN]	Fz [kN]	Fx [kN]	Fy [kN]	Fz [kN]
Average	-13	1231	2767	-22	1683	2822	-36	758	2644
Standard deviation	85	236	63	87	169	109	197	220	205
Maximum	213	1664	2981	308	2344	3297	697	1646	3375
Minimum	-251	665	2568	-313	1220	2486	-688	18	1823

Fig. 3 shows the results for the 10.7 m/s wind speed. One can notice a small, oscillating load in the transverse direction (X). The largest load is in the axial direction (Z), about 2.8 MN, while the vertical load (Y) is about half of that. All of the loads are unsteady with significant oscillations.

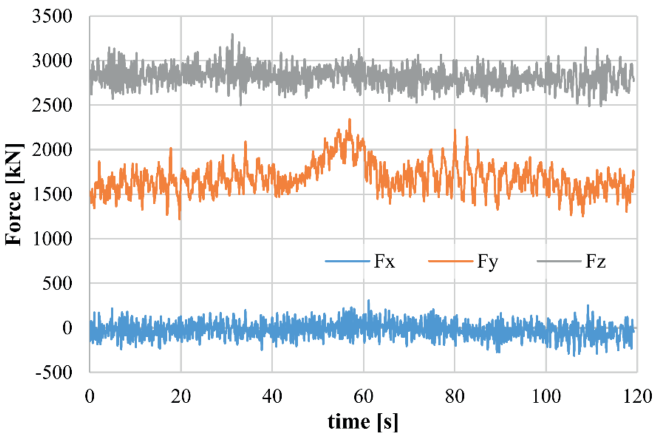

Fig. 3. Force components acting on one of the main bearings for the case with a wind speed of 10.7 m/s

Direct data from the literature may also be used to gain insight into the loads exerted on the main bearing of a wind turbine. In [38], the authors used the following data as the load of the studied tilting pad journal bearing: a radial load of up to 800 kN, and a rotor speed of 10 RPM. The bearing size was 1.4 m x 0.47 m (D x B), which results in a bearing specific load of 1.21 MPa and a sliding speed of 0.7 m/s.

Similar bearing data and loads were used in a recent paper by the same authors dealing with a special bearing arrangement of a 6 MW wind turbine [39].

The other set of data that can be used was presented by Kock et al. [7]. Data for a 6 MW wind turbine were calculated with the use of the multi-body system simulation framework presented in [40], taking into account the flexibility of all relevant structural elements of the wind turbine. The maximum loads for a specific time step (thrust up to 1.4 MN, radial force up to 1.1 MN, and bending moments up to 900 kNm), during the start-up operation, have been selected for the determination of the main bearing load distribution, and as a result, a vertical component of the radial load of 1145 kN was determined, with a very small horizontal component. For a bearing diameter of 1.5 m with an L/B ratio of 0.5 and a bearing length equal to 0.75 m, the sliding bearing specific load is equal to 1.1 MPa. A rotor rotational speed of 12.1 RPM results in a sliding speed of approximately 0.9 m/s.

The literature and our own data concerning bearing operating conditions are collected in Table 3; on this basis, the test conditions were selected.

Tab. 3. Operating parameters of wind turbine bearings from HAWC2 simulations and the literature

Parameter	Units	HAWC2	Kock et al. [7]	Zhang et al. [22, 38]
Turbine rated power	MW	15	6	6
Bearing radial load	kN	Up to 2350	1145	800
Main shaft rotational speed	RPM	7.6	12.1	10
Assumed bearing size (d x B)	m	2.2 x 1.1	1.5 x 0.75	1.4 x 0.47
Bearing specific load	MPa	0.97	1.1	1.2
Bearing sliding speed	m/s	0.8	0.9	0.7

EXPERIMENTAL BEARING TESTS

Assuming that offshore wind turbines will be subject to environmental impact requirements similar to those of ships, the task was to examine bearing materials that are accepted by global marine classification societies.

Based on available knowledge, it is known that it is advisable for the bearing design to enable the replacement of wearing elements in the wind turbine nacelle by an appropriately trained service team. Therefore, the sliding couple must be designed so that the shaft journal wear is minimised and remachining (grinding or turning) will not be necessary.

Experiments were carried out on a model bearing with a diameter of 100 mm, in conditions as close as possible to those in a real wind turbine, which means that the sliding speeds and the specific load in the test bearing and the real object are similar, but for water lubrication conditions.

A specialised test stand was used for experimental tests (Fig. 4). The electric motor integrated with the reduction gear, controlled by the AC controller, drives the main shaft of the test rig (1). The tested journal bearing unit (2) was mounted on the shaft. The tested bearing was closed on both sides by covers with seals. The radial load is applied by a hydraulic cylinder (4). To be able to measure the friction torque of the tested bearing assembly, the radial load is exerted by a hydrostatic radial bearing. In order to be able to more accurately assess the value of the measured resistance to movement of the tested bearing, a module equipped with two sealing rings (5) was placed on the main shaft, which makes it possible to compensate for the friction exerted by the seals in the tested bearing unit (2). Freshwater is pumped through the tested bearing assembly (2) and the seal module (5), and it lubricates and removes heat from the friction zone. The details are presented in Table 4.

Tab. 4. Bearing operational conditions and details of measurement system

Shaft rotational speed [rps]	0.16–3
Linear sliding speed [m/s]	0.05–1
Radial load [N]	6 kN, 9 kN, 12 kN
Specific load [MPa]	0.6 MPa, 0.9 MPa, 1.2 MPa
Friction torque measurements based on the measurement of the force acting on an arm of 0.2 m length – strain gauge sensor with an amplifier, range 0–100 N, accuracy ±0.5% FS	
Temperature measurements – K thermocouples, accuracy 1% FS	
A/D data acquisition system, PC, and A/D card	

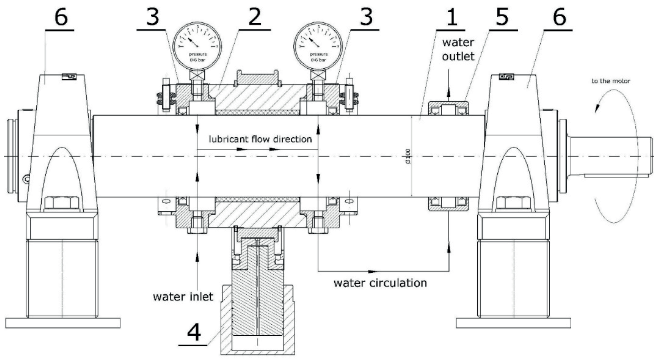

Fig. 4. The test rig. 1 – 100-mm-diameter main shaft, 2 – steel sleeve with tested bearing bush installed inside, 3 – covers with lip sealings, 4 – radial load hydraulic jack, 5 – two lip seals module for measuring seal friction torque, 6 – guiding main shaft, self-alignment ball bearings

Experimental tests were carried out for four different bushing materials; the material data are presented in Table 5. As mentioned before, material selection included materials compliant with water lubrication. The first bearing was fitted with a bush made from lignum vitae material, traditionally used in marine applications for stern tube bearings. This material is of a natural origin, and it has a long history of marine applications and also prospects for increased use in the future, driven by environmental regulations limiting the use of PFAS-containing polymers [40–42]. The second bearing was manufactured from an elastic, relatively soft material, also used extensively in marine applications. The third tested bearing had a bush of a composite three-layer material. The material

Tab 5. Selected material properties of investigated bearings

	Units	Bearing 1	Bearing 2	Bearing 3	Bearing 4
Manufacturer/material		Wood – Lignum vitae	Elastic polymer	3 layer	Composite
Material type		Natural wood	Elastomer	PTFE/NBR/ Bronze	Composite with fibres
Modulus of elasticity (radial direction)	MPa	8000-14000	440-600	PTFE – 770 NBR – 40 Bronze – 103000	22025
Thermal expansion coefficient	10^{-5} 1/K	Radial: 0.3–1 Along rings: 2–3	Non-linear: below 0°C - 10.9 0<T<30°C – 15.1 over 30°C – 21.1	PTFE – 12.4 NBR – 17 Bronze – 2.2	$6 \cdot 10^{-5}$
Thermal conductivity coefficient	W/K·m	0.13	0.25	PTFE – 0.19 NBR – 0.25 Bronze - 50	0.55
Water swell	%	Along ring: 0.5 Radial: 5 Volumetric: 6.3	1.3	PTFE – 0 NBR – 0 Bronze - 0	0.1
Maximum temperature of operation	°C	Unknown	60	PTFE – 120	130
Melting point	°C	-	-	PTFE ~ 260 (decomposition)	-

layout comprises PTFE for a thin sliding layer, combined with rubber as a second layer, and a solid bronze bush. The fourth bearing was made from a polymer reinforced with fibres. The bearing clearance for all tested cases was in the range of 0.2–0.3 mm. Before the tests, each of the tested bearings went through a running-in process lasting several hours, where the sliding speed was gradually reduced for the assumed loads of 0.6 MPa and then 0.9 MPa. The tests themselves were run with a stepwise decrease of the rotational speed starting from 3 rps and ending with 0.16 rps – a sliding speed from 1–0.05 m/s. Each test was repeated three times.

The test bearings are shown in Fig. 5. The lignum vitae bush is dismounted from the steel housing, while the other three bearings are shown in the housing. The bearings were manufactured according to manufacturers' recommendations, including the different arrangements of the lubricating grooves. In all cases, however, the loaded lower half of the bearing circumference has the same cylindrical shape.

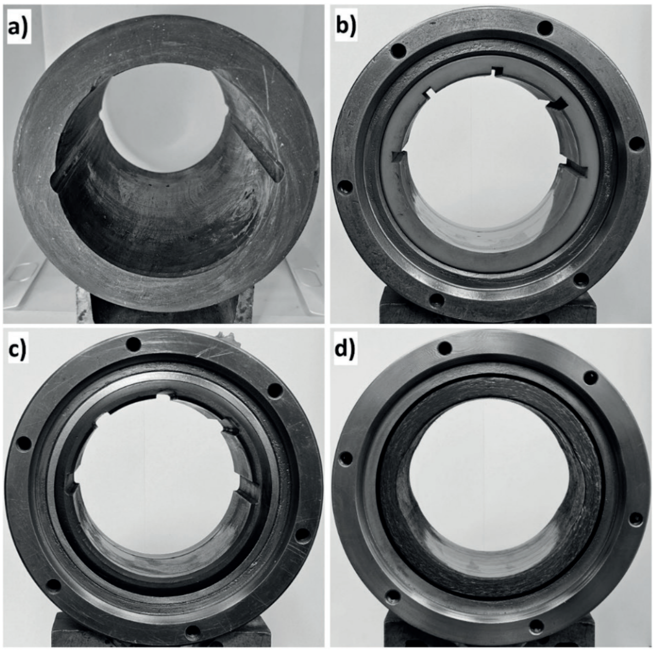

Fig. 5. Tested bearing bushes: a) lignum vitae bush dismounted from the steel housing, b) elastic polymer, b) three-layer, c) fibre-reinforced composite

RESULTS

The results are presented in the form of graphs showing the friction force and coefficient of friction as a function of the rotational speed, respectively, for the lignum vitae bearing (Fig. 6), elastic polymer bearing (Fig. 7), three-layer bush (Fig. 8), and fibre-reinforced composite (Fig. 9).

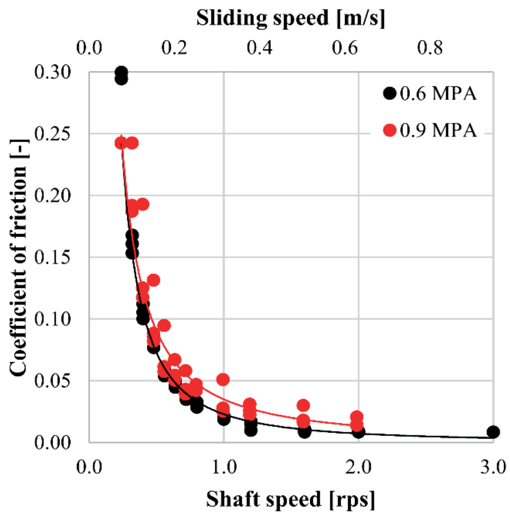

Fig. 6. Friction coefficient in a lignum vitae bearing

In the lignum vitae bearing, the bush value of the friction coefficient was quite high at the lowest speed (COF = 0.3) and dropped to the minimum value at a speed of 1 rps. There are differences between the two loads – at a load of 0.9 MPa and at medium speeds, the coefficient of friction is higher than that at 0.6 MPa.

In the bearing made from the elastic polymer, the friction coefficient was very low at the lowest speed (COF = 0.075) and dropped significantly. It reached a value of 0.05 at 0.5 rps. The coefficient of friction did not change significantly with increasing rotational speed. At all three tested specific loads, the coefficient of friction was very similar.

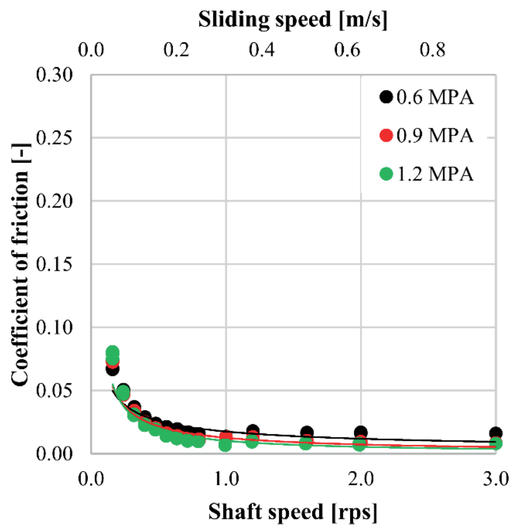

Fig. 7. Friction coefficient in a bearing with elastic polymer

The bearing made from a three-layer composite had an initial friction coefficient that was also low (approx. 0.1) and dropped below 0.025 at a speed of 0.75 RPM; it stabilised at the lowest value after reaching a speed of 1.5 m/s. As with the three-layer composite, at all three tested specific loads, the coefficient of friction was very similar.

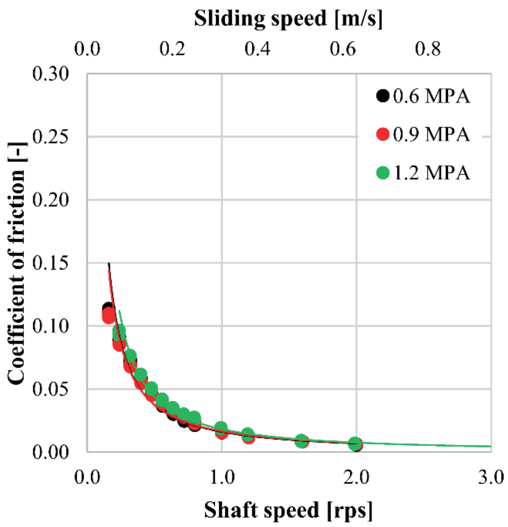

Fig. 8. Friction force and friction coefficient in a bearing with three-layer composite

In the bearing with the bush made from a fibre-reinforced polymer, the initial friction coefficient was quite high (approx. 0.25) and did not drop quickly with increasing rotational speed. At different loads, the friction coefficient was different, with a high load yielding a bigger friction coefficient, which dropped to lower values only at higher speeds.

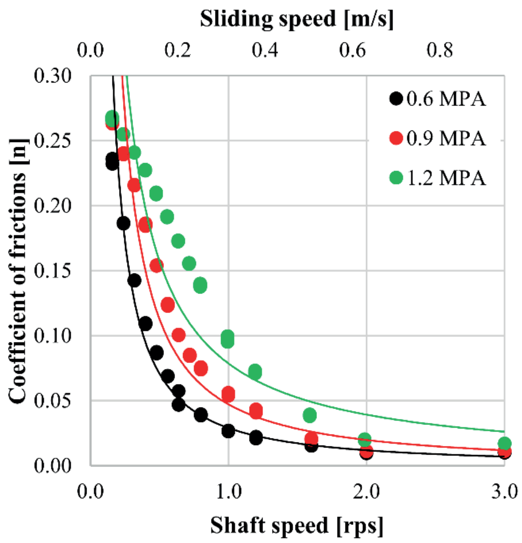

Fig. 9. Friction force and friction coefficient in a bearing with fibre-reinforced composite

The bearings demonstrated a different behaviour with decreasing speed. Although at the maximum rotational speed used in the tests, in all four bearings, the coefficient of friction was similar and well below 0.025, at lower speeds, it differed greatly. In the bearing with the bush made from a fibre-reinforced composite, the value of the friction coefficient remained high and dropped to a minimum value only at the highest rotational speed, which may show that the full hydrodynamic lubrication regime was only possible at a sliding speed exceeding 0.5 m/s. Also, in the bearing with the lignum vitae bush, the friction coefficient at low speeds was high and did not drop drastically with increasing speed; values close to the minimum were obtained at a sliding speed above 0.3 m/s. The other two bearings (elastic polymer and three-layer composite) showed better performance, characterised by lower friction coefficients at low rotational speeds – 0.075 and 0.11, respectively. The decrease of the friction coefficient at higher speeds also occurred at lower rotational speeds, which shows that a full film lubrication regime was obtained at lower rotational/sliding speeds.

In order to compare all four materials, friction coefficients at high speed (2 rps) and at low speed (0.24 rps) are compared in Fig. 10 and Fig. 11. One can see that the friction coefficient does not exceed 0.02 for all bearings, with that of the three-layer bearing being equal to approximately 0.005. At low rotational speeds, the friction coefficients of particular materials differ, with lignum vitae and composite bearings having friction coefficients larger than 0.2, while three-layer bearings and composite bearings have friction coefficients below 0.1.

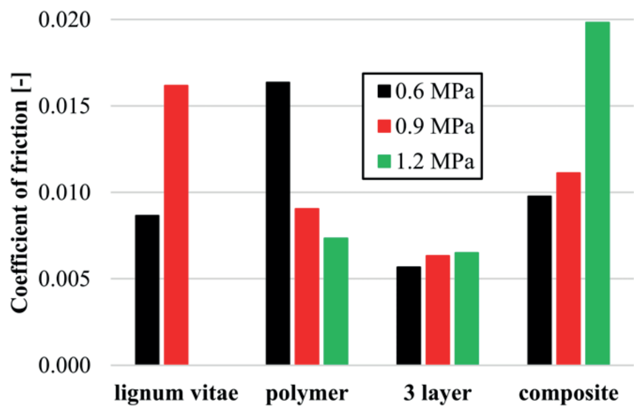

Fig. 10. Friction coefficients of the tested bearings at high rotational speed – 2 rps (0.63 m/s)

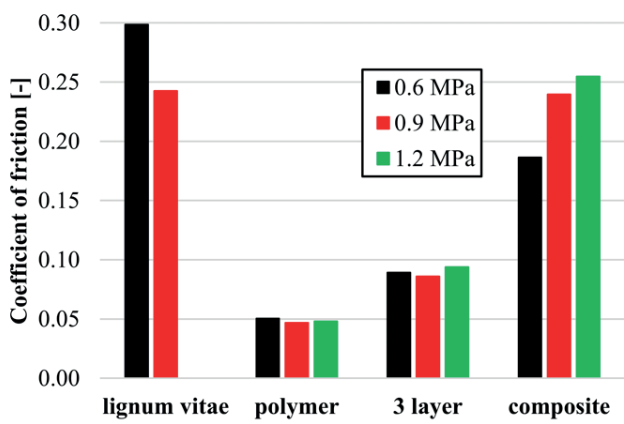

Fig. 11. Friction coefficients of the tested bearings at low rotational speed – 0.24 rps (0.075 m/s)

SUMMARY AND CONCLUSIONS

The results of representative tests of four radial sliding bearings made from different materials compliant with water lubrication showed that there are bearing materials that can be used for slider bearings for the main shaft bearings of wind turbines. The other criterion for selecting materials for the tests was their compliance with and the potential for operation in misaligned conditions caused by shaft bending or nacelle frame deformations. In this aspect, because of possible deformations and a heavy rotor supported on the shaft beyond the bearing support, the wind turbine application is to some extent similar to a ship propeller bearing, and it is no surprise that the selected materials are also the choice for water-lubricated stave bearings.

Experimental tests were conducted using a custom test rig to evaluate the friction performance of journal bearings made from four different water-lubricated bushing materials. The setup enabled the precise measurement of friction torque under controlled radial loads and included a seal compensation module to isolate the bearing friction. Freshwater was used for lubrication and cooling. The tested materials included lignum vitae, a soft elastic polymer, a three-layer composite with PTFE, and a fibre-reinforced polymer. All bearings underwent a running-in process before testing, which involved stepwise speed reduction under fixed loads, and each test was repeated three times for consistency.

The key conditions for the experiment – the sliding speed and load – were determined based on a hybrid approach. On the one hand, a HAWC2 multi-body simulation of an IEA 15 MW wind turbine was performed, and the radial bearing loads were calculated for selected operating conditions. On the other hand, loading was calculated based on the results from the literature survey. Both methods resulted in a consistent maximum load assessment, which was later used in the test section.

The experimental tests were performed to investigate the viability of the use of the tested materials to support the radial load in a main bearing of a large wind turbine. The advantages of sliding bearings in comparison to rolling element bearings are widely known, and in wind turbine applications, better accommodation of dynamic loading and resistance to corrosion may be the most important, potentially leading to longer life, which was discussed in more detail in the introduction section.

The results of the representative testing of four sliding bearings made from different materials compliant with water lubrication showed that there are bearing materials that can be used for slider bearings for main shaft bearings for offshore wind turbines. Out of the tested materials, the polymer and three-layer bearings presented very good performance with very low friction coefficients both at a higher (nominal) rotational speed and also during the start-up phase. In nominal conditions, the bearings were operating in a full film lubrication regime, based on the measurement of a very low friction coefficient. A full film lubrication regime, in which the shaft and bush are fully separated by lubricant film, may have the potential to provide a low wear rate and high durability for the bearings. After the tests, the bearing surfaces in all four bushes were in good condition, showing only the marks of the running-in process, with neither measurable wear nor any destruction.

The described tests were an initial step leading to further investigation, which should include the following:

- A more detailed study on wear behaviour, including start-up and stopping conditions;
- A study of the bearing's starting torque;
- A study of the bearing's operation in misaligned conditions;
- A separate study addressing the accommodation of the thrust load in a separate thrust bearing or in a combined thrust-radial bearing.

Another direction for further research could be the inclusion of other environmentally acceptable lubricants with higher viscosity, such as EAL lubricating oils, which may have a higher potential of generating thicker lubrication films, i.e. lower wear with environmental safety.

ACKNOWLEDGEMENT:

The research was carried out within the project CETP/2022/49/HYBRID WIND/2024, financed by the National Centre for Research and Development, Poland

REFERENCES

1. Nejad AR, et al. Wind turbine drivetrains: state-of-the-art technologies and future development trends. Wind Energ Sci 2022, 7, 387–411. https://doi.org/10.5194/wes-7-387-2022.

2. Zhu C, Zhang R, Song C, Tan J, Yang L. Research status and development trends of large wind turbine main shaft sliding bearings. China Mech Eng 2024, 35(10), 1711–1721. https://doi.org/10.3969/j.issn.1004-132X.2024.10.001.

3. Liu Z, Zhang L. A review of failure modes, condition monitoring and fault diagnosis methods for large-scale wind turbine bearings. Meas 2020, 149, 107002. https://doi.org/10.1016/j.measurement.2019.107002.

4. Hart E, et al. Main bearing replacement and damage – A field data on 15 gigawatts of wind energy capacity. Natl Renew Energy Lab, NREL/TP-5000-86228, 2023. Retrieved from https://www.nrel.gov/docs/fy23osti/86228.pdf.

5. Liang Y, An Z, Liu B. Fatigue life prediction for wind turbine main shaft bearings. Int Conf Qual, Reliab, Risk, Maint, Safety Eng (QR2MSE), 2013. https://doi.org/10.1109/QR2MSE.2013.6625711.

6. Yuan Y, Wang J, Ren L, Chen J. Influence of axial clearance on load distribution in double supported tapered roller bearings of wind turbine main shaft. Proc Inst Mech Eng

C J Mech Eng Sci 2024, 238(21), 10536–10552. https://doi.org/10.1177/09544062241266069.

7. Kock S, Jacobs G, Bosse D. Determination of wind turbine main bearing load distribution. J Phys Conf Ser 2019, 1222, 012030. https://doi.org/10.1088/1742-6596/1222/1/012030.

8. AL-Bedhany JH, Mankhi TA, Legutko S. A surface study of failed planetary wind turbine gearbox bearings to investigate the causes of the bearing premature failure issue. Heliyon 2024, 10(4), e25860. https://doi.org/10.1016/j.heliyon.2024.e25860.

9. Kenworthy J, et al. Wind turbine main bearing rating lives as determined by IEC 61400-1 and ISO 281: a critical review and exploratory case study. Wind Energy 2024, 27(2), 179–197. https://doi.org/10.1002/we.2883.

10. Cheng S, Meng X, Yin J, Yang L, Zhang J. Configuration performance of main shaft bearings for transient-loaded wind turbine. Int J Mech Sci 2025, 293, 110171. https://doi.org/10.1016/j.ijmecsci.2025.110171.

11. Ding H, Mermertas Ü, Hagemann T, Schwarze H. Calculation and validation of planet gear sliding bearings for a three-stage wind turbine gearbox. Lubricants 2024, 12, 95. https://doi.org/10.3390/lubricants12030095.

12. Hirani H. Fundamentals of engineering tribology with applications. Cambridge University Press; 2016. https://doi.org/10.1017/CBO9781107479975.

13. Khonsari MM, Booser ER. Applied tribology: bearing design and lubrication. Wiley-Interscience; 2017. https://doi.org/10.1002/9781118700280.

14. Euler J, Jacobs G, Loriemi A, Jakobs T, Rolink A, Röder J. Scaling challenges for conical plain bearings as wind turbine main bearings. Wind 2023, 3, 485–495. https://doi.org/10.3390/wind3040027.

15. Larsen TJ, Hansen AM. How 2 HAWC2: the user's manual (Risoe-R-1597). Forskningscenter Risoe; 2007.

16. U.S. Environmental Protection Agency. Vessel General Permit for Discharges Incidental to the Normal Operation of a Vessel (VGP), 2013.

17. U.S. Environmental Protection Agency. The Vessel Incidental Discharge Act (VIDA), 2018.

18. Orndorff R. Water lubricated rubber bearings, history and new developments. Nav Eng J 1985, 39–52. https://doi.org/10.1111/j.1559-3584.1985.tb01877.x.

19. Litwin W. Experimental research on water lubricated three layer sliding bearing with lubrication grooves in the upper part of the bush and its comparison with a rubber bearing. Tribol Int 2015, 82, 153–161. https://doi.org/10.1016/j.triboint.2014.10.002.

20. Carter CD. Seawater for propeller shaft lubrication in merchant ships - environmental, operational, legal and shipbuilding considerations. World Maritime Technology Conf, 2024. https://thordonbearings.com/docs/default-source/marine/technical-papers/seawater-for-propeller-shaft-lubrication-in-merchant-ships.pdf?sfvrsn=6d500b85_22.

21. Olszewski A, Żochowski T, Gołębiewski G. Analysis of the load-carrying capacity of a hydrodynamic water-lubricated bearing in a hydroelectric power plant. Tribologia 2018, 2, 103–110. https://doi.org/10.5604/01.3001.0012.6982.

22. Zhang R, Song C, Zhou Y, Tan J, Zeng Z. Tribodynamic behavior of a novel double bearing layout for the main shaft system of wind turbines. Tribol Int 2024, 195, 110496. https://doi.org/10.1016/j.triboint.2024.110496.

23. SKF. Wind turbine main shaft bearing design considerations, 2019. Retrieved from https://www.skf.com/ph/news-and-events/news/2019/2019-10-08-wind-turbine-main-shaft-bearing-design-considerations.

24. Hart E, Turnbull A, Feuchtwang J, McMillan D, Golysheva E, Elliott R. Wind turbine main-bearing loading and wind field characteristics. Wind Energy 2019, 22, 1534–1547. https://doi.org/10.1002/we.2386.

25. Eggers AJ, Digumarthi R, Chaney K. Wind shear and turbulence effects on rotor fatigue and loads control. J Sol Energy Eng 2003, 125(4), 402. https://doi.org/10.1115/1.1629752.

26. Cardaun M, Roscher B, Schelenz R, Jacobs G. Analysis of wind-turbine main bearing loads due to constant yaw misalignments over a 20 years timespan. Energies 2019, 12, 1768. https://doi.org/10.3390/en12091768.

27. Brand AJ, Peinke J, Mann J. Turbulence and wind turbines. J Phys Conf Ser 2011, 318, 072005. https://doi.org/10.1088/1742-6596/318/7/072005.

28. Lee S, Churchfield M, Moriarty P, Jonkman J, J. Michalakes J. Atmospheric and wake turbulence impacts on wind turbine fatigue loadings. AIAA 2012-540, 50th AIAA Aerosp Sci Meet, 2012. https://doi.org/10.2514/6.2012-540.

29. Krathe VL, Thedin R, Jonkman JM, et al. Main bearing response in a waked 15-MW floating wind turbine in below-rated conditions. Forsch Ingenieurwes 2025, 89, 37. https://doi.org/10.1007/s10010-025-00808-z.

30. Heege A, Hemmelmann J. Matching experimental and numerical data of dynamic power train loads by modeling of defects. Wind Energy 2015, 18, 541–558. https://doi.org/10.1002/we.1711.

31. Sethuraman L, Guo Y, Sheng S. Main bearing dynamics in three-point suspension drivetrains for wind turbines. NREL, AWEA WINDPOWER, Orlando, FL, 2015. Retrieved from https://docs.nrel.gov/docs/fy15osti/64311.pdf.

32. Gaertner E, et al. Definition of the IEA 15-megawatt offshore reference wind turbine (NREL/TP-5000-75698), NREL, 2020. Retrieved from https://www.nrel.gov/docs/fy20osti/75698.pdf.

33. WISDEM. WISDEM software, GitHub, 2024. Retrieved from https://github.com/WISDEM/WISDEM.

34. International Electrotechnical Commission. IEC 61400-1: Wind turbines – Part 1: Design requirements, 2019, ed. 4.0.

35. Mann J. Wind field simulation. Probabilist Eng Mech 1998, 13(4), 269–282. https://doi.org/10.1016/S0266-8920(97)00036-2.

36. Liew J. jaimeliew1/Mann.rs: Publish Mann.rs (v1.0.0), Zenodo, 2022. https://doi.org/10.5281/zenodo.7254149.

37. Hansen MH, Henriksen LC. Basic DTU Wind Energy Controller (DTU Wind Energy Report E-0018), DTU Wind Energy, 2013.

38. Zhang R, Song C, Zhou Y, Tan J, Zeng Z. Dynamic performances of novel misaligned non-uniform distributed tilting-pad bearing. Int J Mech Sci 2024, 289, 109020. https://doi.org/10.1016/j.ijmecsci.2024.109020.

39. Jassmann U, Pausch M, Fischer F, Krebs M. Model predictive control of a wind turbine modelled in Simpack. J Phys Conf Ser 2014, 524, 012047. https://doi.org/10.1088/1742-6596/524/1/012047.

40. Branagan L. Water lubricated bearings with lignum vitae: environmentally sound choice. 18th EDF/Pprime Workshop, 2019.

41. Dong C, Zhou X, Yan L, Zhang Y. Effects of anisotropy of lignum vitae wood on its tribological performances. Compos B Eng 2022, 228, 109426. https://doi.org/10.1016/j.compositesb.2021.109426.

42. Wu Z, Zhu Y, Li J, Zhang H. Lignum vitae wood-derived composites for high lubricating performance. J Clean Prod 2023, 406, 137086. https://doi.org/10.1016/j.jclepro.2023.137086.